Revision Submitted to the Journal of Quaternary Science Reviews
October 19, 2017

The Role of Sediment Compaction and Groundwater Withdrawal in Local Sea-Level Rise, Sandy Hook, New Jersey, USA

Christopher S. Johnson,[a,b*] Kenneth G. Miller,[a,b] James V. Browning,[a,b] Robert E. Kopp,[a,b,c] Nicole S. Khan,[d,e,f] Ying Fan,[a,b] Scott D. Stanford,[g] and Benjamin P. Horton[b,d,e,f]

[a]*Department of Earth and Planetary Sciences, Rutgers University, 610 Taylor Road, Piscataway, New Jersey 08854, USA; *Corresponding author, E-mail: c.s.johnson@rutgers.edu*

[b]*Institute of Earth, Ocean and Atmospheric Sciences, Rutgers University, 71 Dudley Road, New Brunswick, New Jersey 08901, USA*

[c]*Rutgers Energy Institute, Rutgers University, 71 Dudley Road, New Brunswick, New Jersey 08901, USA*

[d,]*Sea Level Research, Department of Marine and Coastal Sciences, Rutgers University, 71 Dudley Road, New Brunswick, New Jersey 08901, USA*

[e]*Earth Observatory of Singapore, Nanyang Technological University, 50 Nanyang Avenue, Singapore 639798, Singapore*

[f]*Asian School of the Environment, Nanyang Technological University, 50 Nanyang Avenue, Singapore 639798, Singapore*

[g]*New Jersey Geological and Water Survey, P.O. Box 420, Trenton, New Jersey 08625-0420, USA*

Key Words

Quaternary, Sea-level Change, North America, Sedimentology, Marginal Marine, Numerical Modeling

Highlights

- We quantify subsidence at Sandy Hook to determine the effects of natural and anthropogenic sources causing high local rates of sea-level rise.
- We develop a single decompaction equation describing porosity as a function of grain size, burial depth, and age applicable to other regions.
- Compaction of Quaternary organic material has a negligible contribution, whereas compaction of fine-grained siliciclastic sediments is causing 0.16 mm/yr (90% C.I., 0.6-0.32 mm/yr) of local sea-level rise.
- Anthropogenic groundwater withdrawal likely contributes the remaining 0.7 mm/yr (90% C. I. 0.3-1.2 mm/yr) of local sea-level rise.

Abstract

The rate of relative sea-level (RSL) rise at Sandy Hook, NJ (4.0±0.5 mm/yr) was higher than The Battery, NY (3.0±0.3 mm/yr) from 1900-2012 despite being separated by just 26 km. The difference cannot be explained by differential glacial isostatic adjustment (GIA; 1.4±0.4 and 1.3±0.4 mm/yr RSL rise, respectively) alone. We estimate the contribution of sediment compaction to subsidence at Sandy Hook using high-resolution grain size, percent organic matter, and porosity data from three late Quaternary (≤13,350 cal yr) cores. The organic matter content (< 2%) is too low to contribute to local subsidence. However, numerical modeling of the grain size-depth-age-porosity relationship indicates that compaction of deglacial silts likely

reduced the column thickness by 10-20% over the past 13,350 cal yrs. While compaction rates were high immediately after the main silt deposition (13,350-13,150 cal yrs BP), rates decreased exponentially after deposition to an average 20th century rate of 0.16 mm/yr (90% Confidence Interval (C.I.), 0.06-0.32 mm/yr). The remaining ~0.7 mm/yr (90% C.I. 0.3-1.2 mm/yr) difference in subsidence between Sandy Hook and The Battery is likely due to anthropogenic groundwater withdrawal. Historical data from Fort Hancock (2 km to the southeast of the Sandy Hook tide gauge) and previous regional work show that local and regional water extraction lowered the water levels in the aquifers underlying Sandy Hook. We suggest that the modern order of contribution to subsidence (highest to lowest) appears to be GIA, local/regional groundwater extraction, and compaction of thick Quaternary silts.

1.0 Introduction

Global, regional, and local processes cause changes in relative sea level (RSL). Global mean sea-level (GMSL) change describes changes in sea surface height averaged over the whole ocean (e.g., Kopp et al., 2015). Due primarily to thermal expansion and shrinking of land ice, GMSL rose at a rate of about 1.4±0.2 mm/yr during the 20th century (Hay et al., 2015; Dangendorf et al., 2017), which is significantly lower than previously published estimates of 1.5-1.9 mm/yr (e.g., Jevrejeva et al., 2008; Church and White, 2011). GMSL has been rising at a rate of about 3 mm/yr from 1993-2014 (Chen et al., 2017). RSL is the vertical distance between sea-surface height and the solid-Earth surface at a specific location (Kopp et al., 2015). RSL may be falling or rising at a different rate from GMSL and can be used to describe sea-level trends for areas on regional (~100 km^2) and local (single location; ~10 km^2) scales. Comparison of RSL rise at Sandy Hook, which lies on thick compressible sediments, and the nearby (26 km) Battery, NY, which lies on incompressible bedrock, provides a natural experiment evaluating the natural and anthropogenic effects on compaction.

The increasing availability of tide-gauge records and geologically based reconstructions of past RSL has made it possible to analyze RSL change with finer spatial resolution (e.g. Kopp, 2013; Kemp et al., 2011; Horton and Shennan, 2009). These analyses have shown it is possible, if not common, to have large variations in rates of RSL change over relatively small (a few kilometers) distances. For example, spatio-temporal statistical analysis of tide-gauge records estimated the rate of RSL rise at Sandy Hook between 1900 and 2012 to be 4.0±0.5 mm/yr (Fig. 2). This rate is significantly higher than the 3.0±0.3 mm/yr observed over the same period at The Battery tide gauge, located just 26 km to the northwest (Kopp, 2013).

RSL change can be influenced by many factors, including glacial isostatic adjustment (GIA; Clark et al., 1978), mantle dynamic topography (e.g., Gurnis, 1990), ocean dynamics (Yin et al., 2009), and local processes including active tectonics (Simms et al., 2016), sediment loading, and compaction (Törnqvist et al., 2008; Brian et al., 2015). Both Sandy Hook and The Battery show 20th century rates greater than the 1.4±0.2 mm/yr of GMSL rise (Hay et al., 2015, Kopp et al., 2016). The excess RSL rise above GMSL rise at these two locations is mainly due to GIA (Clark et al., 1978). Kopp (2013) estimated the GIA effect to be 1.3±0.4 mm/yr at The Battery and 1.4±0.4 mm/yr at Sandy Hook.

Accounting for the difference in GIA between Sandy Hook and The Battery leaves a 0.9 ± 0.5 mm/yr difference in RSL change (Kopp, 2013). This difference cannot be attributed to regional processes, but must be due to unquantified local processes. Moucha et al. (2008) showed that there is little or no difference (≤0.003 mm/yr) in mantle dynamic topography driven RSL change between Sandy Hook and The Battery. Furthermore, changes in ocean dynamics occur over spatial scales too large to affect Sandy Hook and The Battery differently (Yin et al., 2009). Similarly, spatial variation arising from the static-equilibrium (gravitational, rotational, and deformational) effects of shifting mass from land ice to or from the ocean occurs over distances greater than the 26 km between Sandy Hook and The Battery (Kopp et al., 2015). Based on models of long-term thermal subsidence and compaction of pre-Quaternary strata (Kominz et al., 2008), these effects are too low (<0.1 mm/yr difference between sites) to explain the difference (Miller et al., 2013). Thus the 0.9±0.5 mm/yr difference is likely due to sediment compaction.

Here we seek to quantify the sources of local subsidence to account for the high rate of local RSL rise at Sandy Hook. Potential contributors include compaction of organic-rich strata and/or siliciclastic sediments due to natural effects (e.g., Törnqvist et al., 2008) and compaction induced by anthropogenic groundwater withdrawal (e.g., Pope and Burbey, 2004). Locations with high rates of RSL rise (≥~4.0 mm/yr) (e.g. Norfolk, VA and Atlantic City, NJ) are typically the result of high rates of compaction due to groundwater withdrawal (Pope and Burbey, 2004; Cronin, 2012; Miller et al., 2013). In this study, we assess the RSL contributions from compaction of Quaternary organic material and siliciclastic sediments at Sandy Hook. We conduct sedimentological studies (percent organic matter, grain size, and porosity) on a transect of three cores drilled on Sandy Hook (Fig. 1). We use these data to model the contributions of compaction in young unconsolidated siliciclastic silts to local RSL changes and compare the residual to rates of groundwater withdrawal. Our approach to quantify RSL budgets is applicable to other regions.

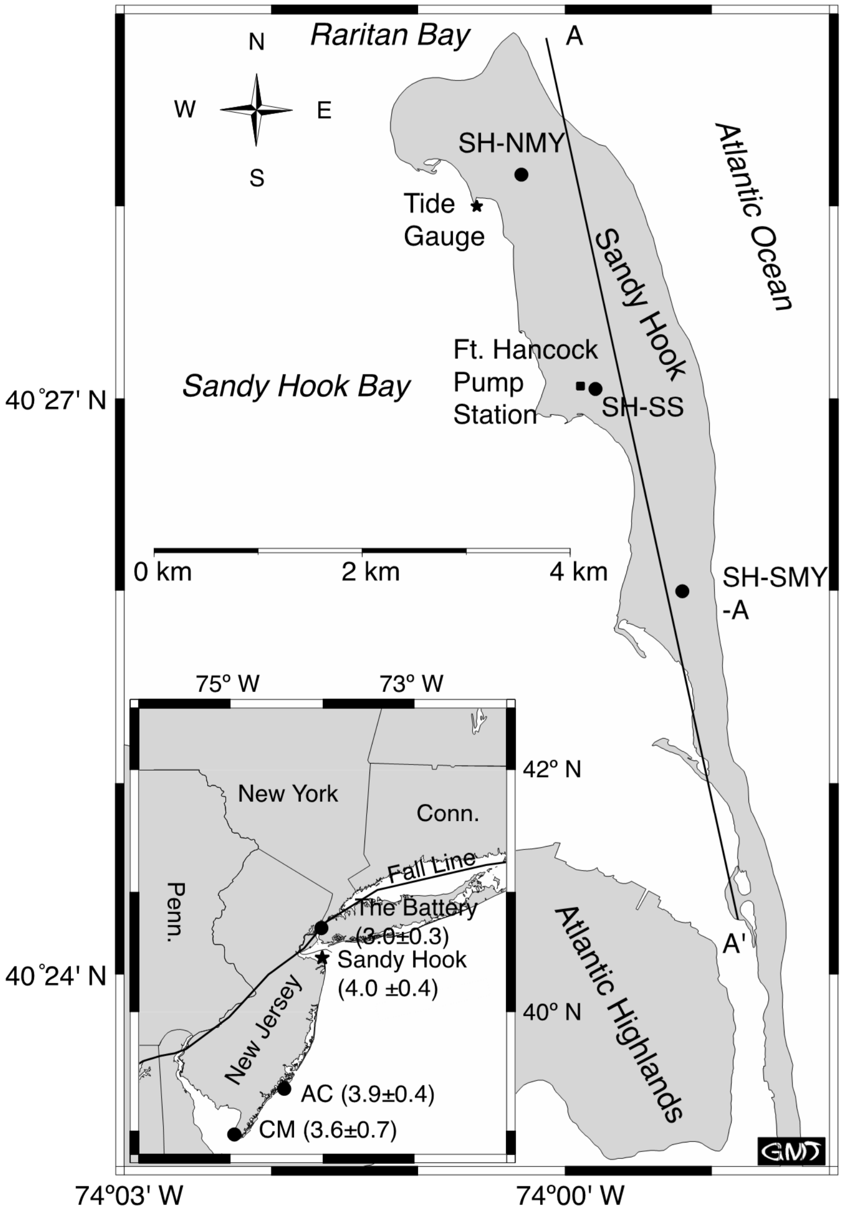

Fig. 1: Sandy Hook Location Map. SH-NMY Sandy Hook North Maintenance Yard Corehole, SH-SS Sandy Hook Salt Shed Corehole, SH-SMY-A Sandy Hook South Maintenance Yard Corehole A. Inset map shows the Fall Line, B = The Battery Tide Gauge, AC = Atlantic City Tide Gauge, CM = Cape May Tide Gauge, and 1900-2012 average rates of sea-level rise at each of those locations including Sandy Hook (Miller et al., 2013). A-A' is the location of the cross-section in Fig. 3.

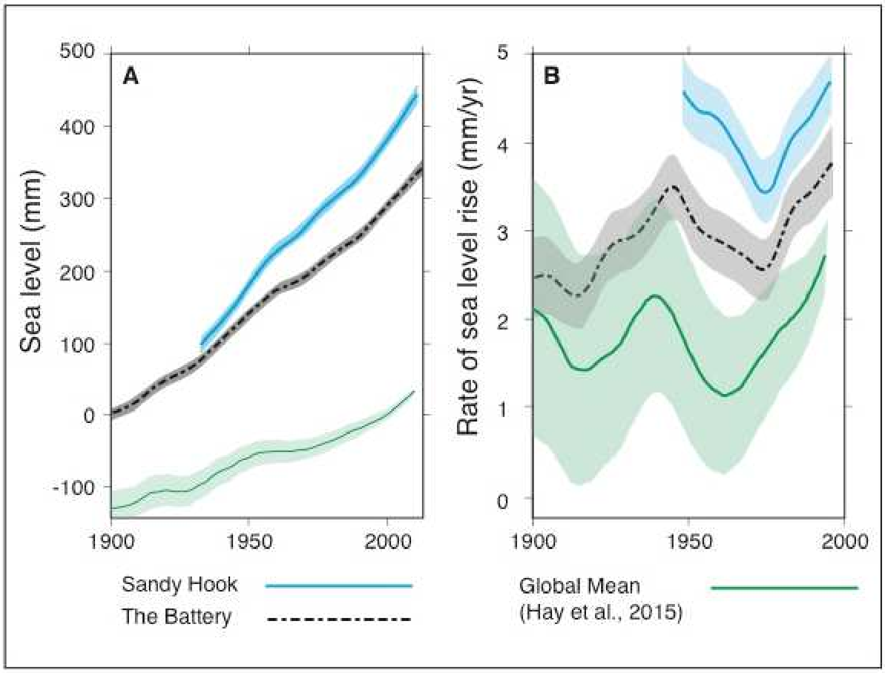

Fig. 2: A: Sea level from tide gauges at Sandy Hook, NJ (cyan) and The Battery, NY (black dashed) compared to the global sea-level curve of Hay et al. (2015) (green). B: 31-year averaged rate of sea-level rise at Sandy Hook (black) and The Battery (blue) compared to global (green; based on data from Hay et al., 2015). Shaded areas are 2σ uncertainty (Modified from Miller et al., 2013).

2.0 Study Area

Sandy Hook is a sand spit extending 8 km north into Sandy Hook and Raritan Bays between New York and New Jersey, USA (Fig. 1). The spit has been growing northward into Raritan Bay at an average rate of ~8 m/yr over the past two centuries (see supplementary material for calculation). The Sandy Hook tide gauge is located near the NW end of the spit, 26 km southeast of The Battery tide gauge in New York, NY. Sandy Hook and The Battery are in different geologic settings. The Battery is underlain by Paleozoic and Proterozoic crystalline metamorphic bedrock (Lyttle and Epstein, 1987), whereas Sandy Hook is in the New Jersey coastal plain underlain by ~300 m of unconsolidated Cretaceous to recent marine, near shore, and terrestrial sediments that onlap the bedrock seaward of the fall line (Owens et al., 1998). The fall line, demarcated by a linear series of waterfalls along rivers traversing the line, marks the transition between unconsolidated sediments and more resistant bedrock to the west (e.g., Owens et al., 1998; Fig. 1).

Miller et al. (2013) used tide gauge records to show that the 20th century regional rate of sea-level rise along the fall line and to the west in the Piedmont is ~3.0 mm/yr. Major cities including New York (3.0±0.3 mm/yr), Philadelphia (3.1±0.3 mm/yr), Baltimore (3.1±0.3 mm/yr), and Washington D.C. (3.0±0.5 mm/yr) are located in this region. These rates closely match the sum of GMSL rise and GIA-driven RSL change. Tide gauges located east of the fall line in the coastal plain typically exhibit rates of rise of at least 3.5 mm/yr and can reach rates as high as 3.9 and 4.0 mm/yr in locations such as Atlantic City, NJ and Sandy Hook, NJ, respectively (Miller et al., 2013) and higher in Virginia (Pope and Burbey, 2004). While the coastal plain sea-level signal includes GMSL rise and GIA similar to the bedrock sites, most coastal plain sites experience an additional 0.5-1.5 mm/yr RSL rise.

3.0 Methods

3.1 Drilling

In order to study the effects of the underlying geology and quantify the contribution of different processes on the local rate of sea-level rise at Sandy Hook, a transect of three continuously cored and logged holes were obtained on a N-S transect (1.6 km apart) on the spit (Miller et al., in press) (Figs. 1, 3, and S1) in 2014 as part of the ongoing Coastal Plain Drilling Project. The three core holes (Figs. 4, 5, and S2) were designated Sandy Hook North Maintenance Yard (NMY) at 40°28.165' N, 74°00.297' W, Sandy Hook Salt Shed (SS) at

40°27.052' N, 73°59.793' W, and Sandy Hook South Maintenance Yard A (SMY-A) at 40° 25.998’ N, 73° 59.202’ W (Miller et al., in press). Basic sediment and stratigraphic descriptions of the cores were done onsite and subsequently along with preliminary interpretations of the depositional environments (Stanford, 2015; Miller et al., in press). Here we provide interpretations along with our new sedimentological data. More detail is provided in the results and discussion.

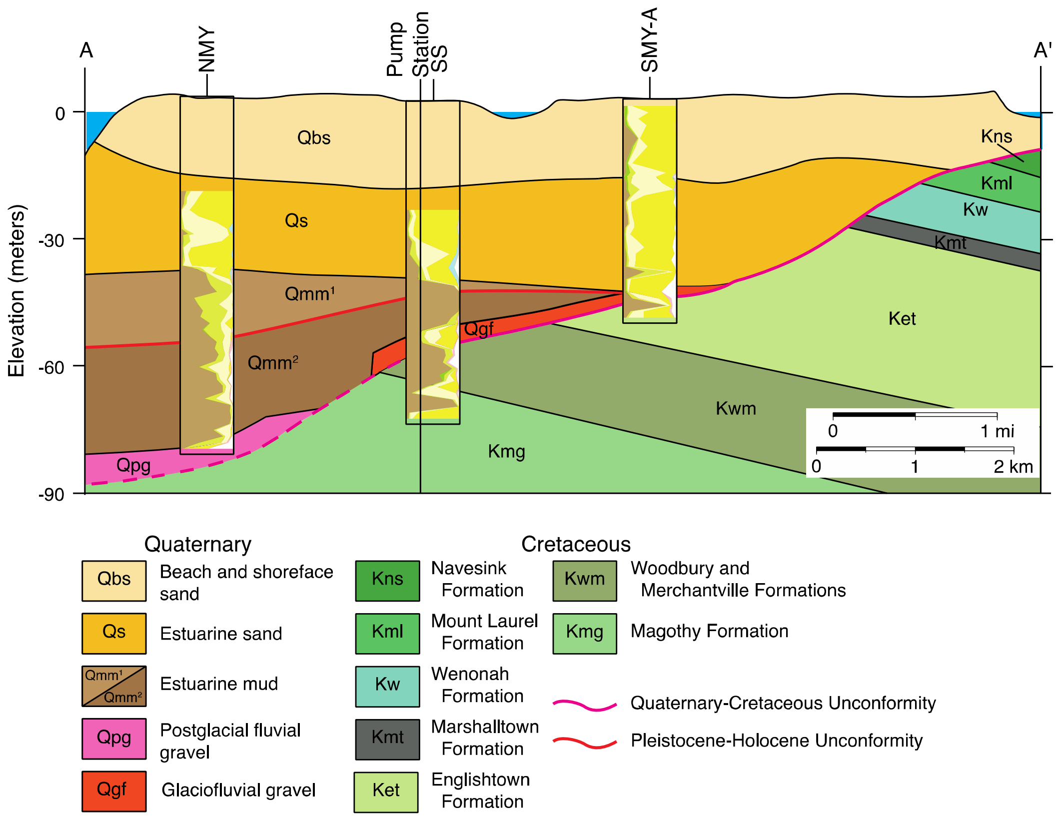

Fig. 3: Schematic cross section of Sandy Hook. Cretaceous sediments are shades of green and Quaternary sediments are shades of yellow. The basal Quaternary postglacial outwash gravel deposit is shown in magenta. Unconformities are marked in red and the inferred glacial incised

valley outline is magenta. The correlation between the gravels at the NMY and SS is based on elevation, provenance, and fluvial grade to outcropping terminal moraines in Staten Island, NY (Miller et al., in press). We follow the nomenclatures of Stanford et al. (2015), and Minard (1969). Modified from Stanford et al. (2015). Cross section location in Fig. 1. Inserts are cumulative percent plots from each of the cores, see Fig. 4 for explanation.

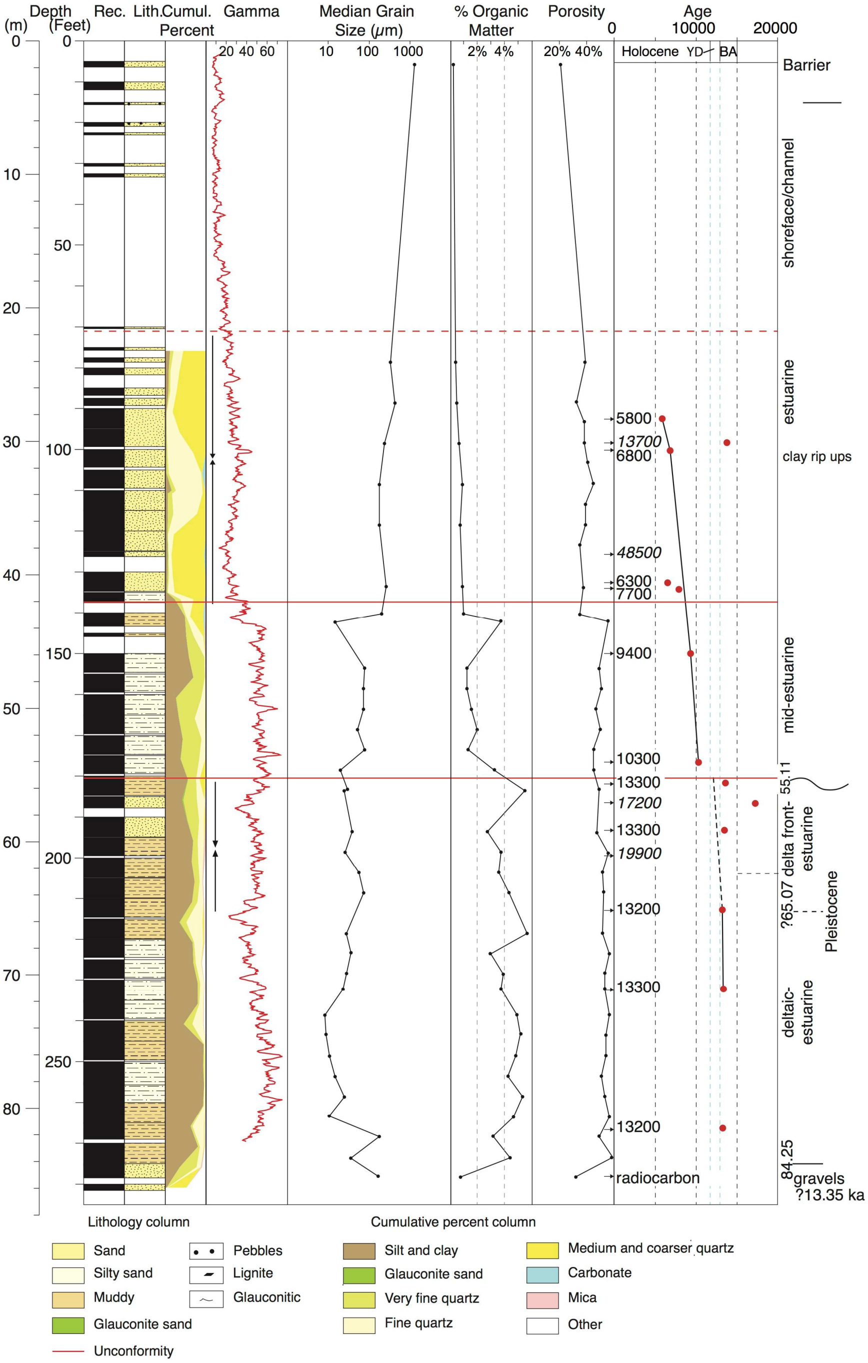

Fig. 4: North Maintenance Yard (NMY) core properties including: recovery, blank spaces indicate unrecovered intervals; lithology; cumulative percent (see key); downhole gamma log; grain size (μm); percent organic matter; porosity; radiocarbon ages in cal years, errors for radiocarbon ages are smaller than data points.

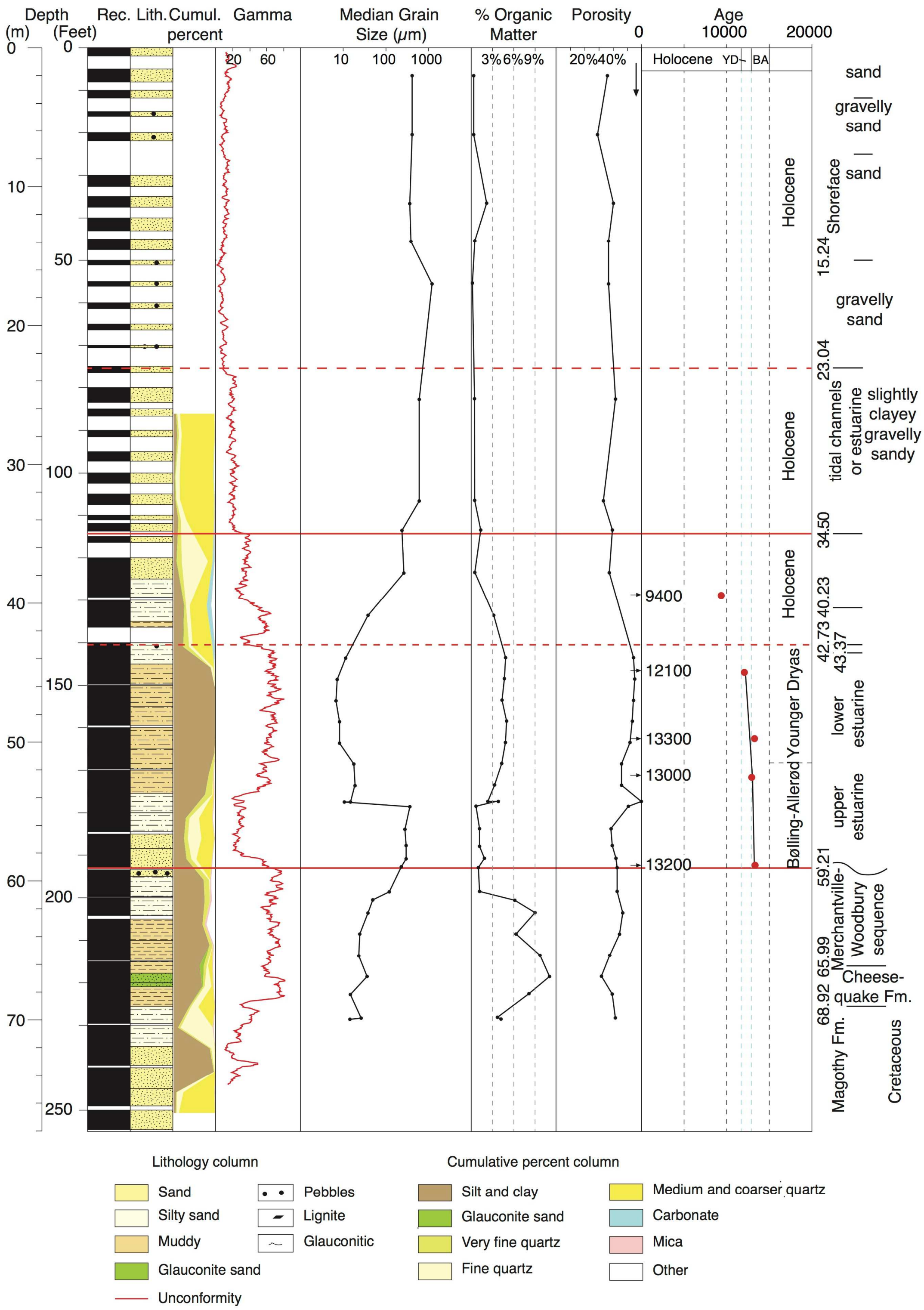

Fig. 5: Salt Shed (SS) core properties including gamma, grain size, %OM, porosity, and age model. See caption for Fig. 4 for details.

3.2 Sedimentological Analyses

We measured percent organic matter (%OM), grain size, radiocarbon ages, and porosity. The lithologic descriptions were synthesized into general lithology columns (Miller et al., in press). We also added quantitative and semi-quantitative lithology data. We quantitatively measured weight percent mud (<63 mm), fine sand (63-125 mm), and medium-coarse sand (>125 mm) in washed samples at ~1.5 m intervals. We semi-quantitatively estimated the abundance of glauconite, shells, and mica in the sand fraction (>63 mm) by splitting samples into aliquots and visually estimating percentages on a picking tray. The semi-quantitative and quantitative percent data were combined and presented as “Cumulative lithology” (Fig. 4, 5, and S1); these clearly show distinct trends in grain size and mineralogy and are particularly useful in showing fining upward and coarsening upward trends not readily observable in the descriptive lithology (e.g., Fig. 4). Where available, samples were taken at ~1.5 m intervals in all silts and ~3 m intervals in the sands, with a higher sample density in zones of rapid sedimentological changes (Table ST1). Percentage organic matter (OM) was measured using loss on ignition, following the method of Heiri et al. (2001), at the Benthic Ecology Lab at Rutgers Department of Marine and Coastal Sciences. The equivalent percent total organic carbon is ~1/2 %OM (Vereş, 2002). Grain size analysis was performed on the <3 mm size fraction using a Malvern Mastersizer 3000 at the Sea Level Research Lab at Rutgers Department of Marine and Coastal Sciences. Radiocarbon dates were acquired using mollusk shells and plant material. Porosity was measured volumetrically, using the mass of pore water to estimate pore volume and the volume of grains to estimate matrix volume. More detailed methods for determining grain size, %OM, and porosity are available in the supplementary material.

3.3 Radiocarbon Ages and Age Models

The Quaternary chronology at Sandy Hook was established using radiocarbon dating, and an age model is developed and presented here in the Methods. The material dated was primarily plant matter, supplemented by shell fragments (Table 1). The shell fragments were mainly *Mercenaria mercenaria*, *Crassostrea virginica*, and indeterminate species. The plant material included wood fragments, peats, and roots; we picked fragile or fresh-looking organic matter that could not have been transported a long distance. All of the dated materials are from facies interpreted as estuarine and equivalent to the modern back bay environments (Raritan and Sandy Hook Bays). Although movement of material in these environments is possible, it does not suffer from the reworking issues of modern and Quaternary shelf and nearshore environments because of rapid deposition at the NMY. The samples were removed from the bulk substrate and adhered detrital material was removed from the sample under a microscope prior to radiocarbon dating.

Lab Number	Sample Depth (m)	Type	^{13}C (‰)	^{14}C Age	Median age (cal yr BP)	Midpoint (cal yr BP)	2 sigma error (from midpoint)	ΔR	ΔR Error	Material Dated
North Maintenance Yard:										
OS-115212	28.22	Plant/Wood	-17.42	5020±25	5771	5775.5	115.5			Leaf and wood fragments
OS-115277	29.98	Plant/Wood	-24.44	11900±30	13728	13683	100			Leaf and wood fragments
OS-115213	30.6	Plant/Wood	-25.51	5990±25	6829	6820.5	71.5			Wood fragments
OS-115278	38.27	Plant/Wood	-29.27	45200±800	48508	48475	1525			Wood fragment
OS-121907	40.44	Mollusk	NM	6050±20	6337	6338.5	132.5	130	60	Shell fragment (indeterminate)
OS-121999	40.9	Plant/Wood	NM	6920±30	7744	7752.5	72.5			Wood fragment
OS-115450	45.74	Mollusk	-0.83	8830±40	9365	9347	164	130	60	Articulated *Mercenaria mercenaria* in shell bed
OS-115453	53.84	Mollusk	-0.87	9580±25	10302	10323.5	152.5	130	60	*Crassostrea virginica* shell
OS-121909	55.41	Plant/Wood	NM	11500±50	13349	13354	102			Small piece of decayed organic matter
OS-115279	56.88	Plant/Wood	-26.65	14150±35	17228	17242.5	182.5			Leaf, wood and charcoal fragments from thin peat unit
OS-121969	58.92	Plant/Wood	NM	11500±65	13347	13335.5	130.5			Small piece of decayed organic matter
OS-121906	60.81	Plant/Wood	NM	16500±95	19902	19886.5	270.5			Fragile detrital organic material
OS-115280	64.9	Plant/Wood	-27.39	11350±30	13194	13196	85			Fragile detrital organic material
OS-115281	70.81	Plant/Wood	-27.33	11450±30	13295	13297	89			Fragile detrital organic material
OS-121908	81.27	Plant/Wood	NM	11300±50	13152	13165.5	96.5			Fragile detrital organic material
OS-115282	84.63	Plant/Wood	-22.8	> 48000±3500						Wood fragments
South Maintenance Yard:										
OS-121910	20.3	Mollusk	NM	4220±15	4136	4146.5	194.5	130	60	Articulated (indeterminate) mollusk in shell bed
OS-121911	23	Mollusk	NM	5450±20	5685	5712	141	130	60	Fragmented (indeterminate) mollusk in shell bed
OS-115287	23.17	Plant/Wood	-28.05	> 48000±0						Bulk peat
OS-115288	23.22	Plant/Wood	-27.26	> 48000±2700						Bulk peat
Salt Shed:										
OS-115283	39.26	Plant/Wood	NM	8350±25	9378	9376.5	77.5			Wood and plant debris
OS-115284	44.7	Plant/Wood	NM	10300±30	12076	12161.5	213.5			Plant fragments and charcoal
OS-115285	52.23	Plant/Wood	-27.24	11100±30	12991	12957.5	114.5			Wood and charcoal fragments
OS-115286	58.61	Plant/Wood	-28.9	11400±30	13241	13228.5	78.5			Fragile detrital organic material
OS-122000	49.59	Plant/Wood	NM	11450±55	13296	13290	133			Fragile detrital organic material

Table 1: Radiocarbon Results. NM=Not Measured

Samples were analyzed at the National Ocean Science Accelerator Mass Spectrometry (NOSAMS) Lab at Woods Hole Oceanographic Institute and the resulting radiocarbon ages calibrated to calendar years using IntCal13 or Marine13 for terrestrial and marine samples respectively (Reimer et al., 2013). A ΔR value of 130 ± 60 was applied to samples determined to form in the marine realm (i.e., marine mollusk and shell fragments) to account for local marine reservoir effects. This ΔR value was obtained from the closest known location available in Shark River, NJ (McNeely et al., 2006).

Age models for the NMY and SS sites were developed using radiocarbon dates and detailed core examination. From 55.11-84.25 m at the NMY, where radiocarbon dates were indistinguishable, we assumed constant deposition across the interval and used the earliest and latest dates (13,347 and 13,152 cal yrs BP) to establish our age model. These dates correlate the silts from 55.11-84.25 m with the Lake Iroquois outburst floods into the Hudson River Valley at 13,350 cal yr BP (Rayburn et al., 2005; Donnelly et al., 2005; Thieler et al., 2007; see discussion). We thus anchor the age model at 13,350 cal yr BP. Above this, we applied linear trend lines to the radiocarbon dates. At points of major (order-of-magnitude) change in deposition rates, we compared the depths of those changes to the depths of potential unconformities in the cores. Where there appeared to be an unconformity, we evaluated the age of the surface of discontinuity from above and below and compared the two ages. The process was repeated for the SS. Error bars were generated using Bacon Version 2.2 (Blaauw and Christen, 2011). More details of the method and the errors are provided in the supplementary material and Figs. S3-S4.

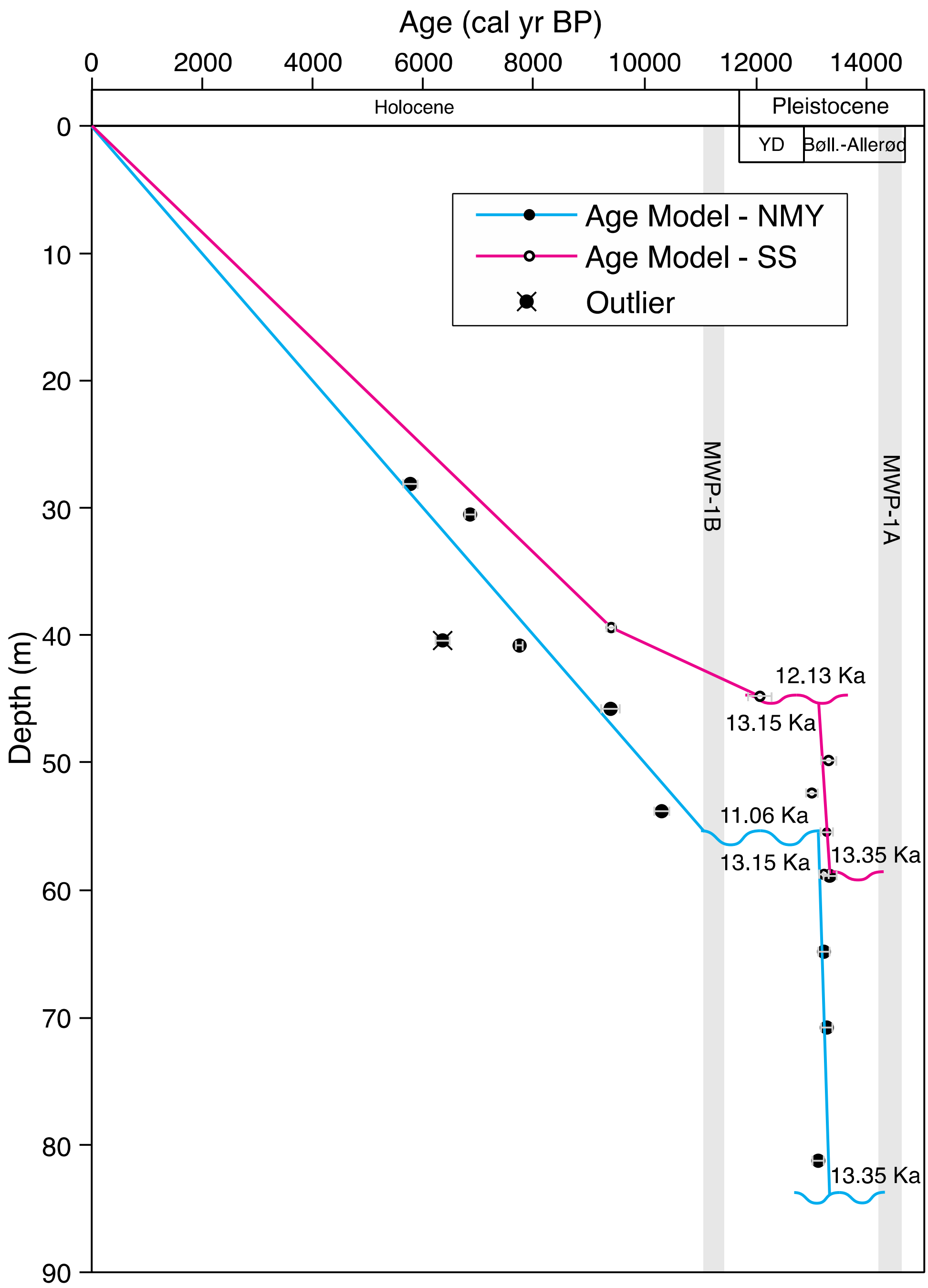

Fig. 6: Age models for NMY and SS sites. Gray bars indicate 2σ uncertainties in the calibrated ages. Dates for events and time periods are from Rasmussen et al., 2006, Deschamps et al., 2012, and Abdul et al., 2016.

3.4 Numerical Modeling

Numerical modeling was employed to quantify the contribution from compaction of siliciclastic sediments to the rate of RSL rise. We sought to decompact the sediment column in discrete time steps. We derived an equation for porosity and used it to model changes in porosity through time and across changes in burial depth.

We tested multiple equations for porosity, changing both the variables of grain size, age, and burial depth controlling porosity and the form of the equation itself. Previously, Kominz et al. (2011) identified strong relationships between grain size and porosity, burial depth and porosity, and age and porosity. We used trends visible in our data set (porosity vs. grain size and porosity vs. depth/age) to design our equations.

Porosity data show a strong logarithmic dependency on median grain size (Fig. S5). Porosities of sands are typically 40%. Quaternary sediments composed primarily of silts had a porosity of ~50-55%. This agrees with the divisions used by Kominz et al. (2011) when describing porosity as a function of depth or age. Even within the silt category (4-63µm), there was a strong dependency of porosity on grain size, with coarser sediments silts having a relatively lower porosity (Figs. 4-5). This may have been, in part, be partly an artifact of dewatering of coarse sections of the core before sampling. Dewatering was clearly visible in the coarsest sediments (coarse sands and gravels). There is also a trend of decreasing porosity in the silts with increasing burial depth/age (Fig. S6), similar to the trend shown by Kominz et al. (2011). This is particularly evident when the Quaternary silts are compared to similar silts in the Cretaceous section underlying the deglacial sediments at the SS. The Cretaceous silts have a porosity of ~40% and are assumed to have been fully compacted. Unlike the results of Kominz et al. (2011), at Sandy Hook, porosity in sands (> 63 μm) did not exhibit a strong relationship with depth or age.

Kominz et al. (2011) also showed that there is greater potential for compaction in finer grained sediments, with young silts having a porosity of ~75% decreasing to a minimum of ~30%. Alternatively, sands start between 45-55% porosity and only decrease to 30% (Kominz et al., 2011). In the coarser Sandy Hook samples, there was very little change in porosity related to changes in burial depth or age that could not be attributed purely to changes in grain size. As such, we assumed that for the time scales seen on Sandy Hook, anything with a median grain size ≥63 μm was relatively incompressible.

Previously, Kominz et al. (2011) employed multiple equations to describe changes in porosity. They separated samples based on grain size into the categories clay, silt, and sand, with separate equations for each. Within each category, they derived two equations, one as a function of depth and another as a function of age. We sought to arrive at a single equation that described porosity (*por*) as a function of grain size in μm (ϕ), burial depth in meters (z), and age in years (a). Using the available data from all three drill sites, Equation 1 was created by regressing the natural logs of median grain size, burial depth, and age against the porosity values (r^2=0.672, Akaike Information Criterion (AIC; an estimator of the relative quality of models for a given set of data)=-115.8796);

$$\mathrm{por} = -0.0158\ln(\phi) - 0.0034\ln(z) - 0.0138\ln(a) + 0.7132 \quad (1)$$

To check our results, we performed a second regression that described porosity as a function of only median grain size and burial depth (Equation 2; r^2=0.348, AIC= -93.8796):

$$\text{por} = -0.0315\ln(\phi) - 0.0350\ln(z) + 0.7385 \quad (2)$$

The inputs used to constrain these equations are available in the supplementary material (Table ST3). A data point taken from the modern upper Hudson River Estuary, with the approximated values of 70% porosity, 10 cm burial depth, and a median grain size of 33.5 μm, was used in the regression to constrain the younger, shallowly buried portion of the curve (Woodruff et al., 2001). Properties of the Cretaceous sediments at the SS site were used to constrain porosities in the older, more deeply buried layers. Due to erosion of overlying sediments, the maximum burial depths for the Cretaceous sediments are unknown and we estimated the values at ~100 m below their current burial depth. The equations do not take sorting into account. This is a potential source of error, as it likely influences the compressibility of the sediments. The average spread of grain sizes (10^{th} percentile to 90^{th} percentile) is ~130 μm at the NMY. The finer sediments tended to have a positive skewness in grain size.

Equations 1 and 2 were used in two separate versions of the numerical model to decompact Sandy Hook at the NMY. The models divide the sediment column into discrete layers and remove them sequentially from the top down, peeling away sediment and time. As each layer is removed, the underlying layers are each decompacted. This is accomplished by calculating the porosity of each layer before removing the top layer and then recalculating the porosity for each layer after the top layer is removed (changing both the burial depth and age of each underlying layer). The change in porosity is then used to calculate a change in thickness for each layer. This process is repeated one layer at a time from the top down in order to account for changes in the thickness of the overlying sediments when calculating the new porosity of each

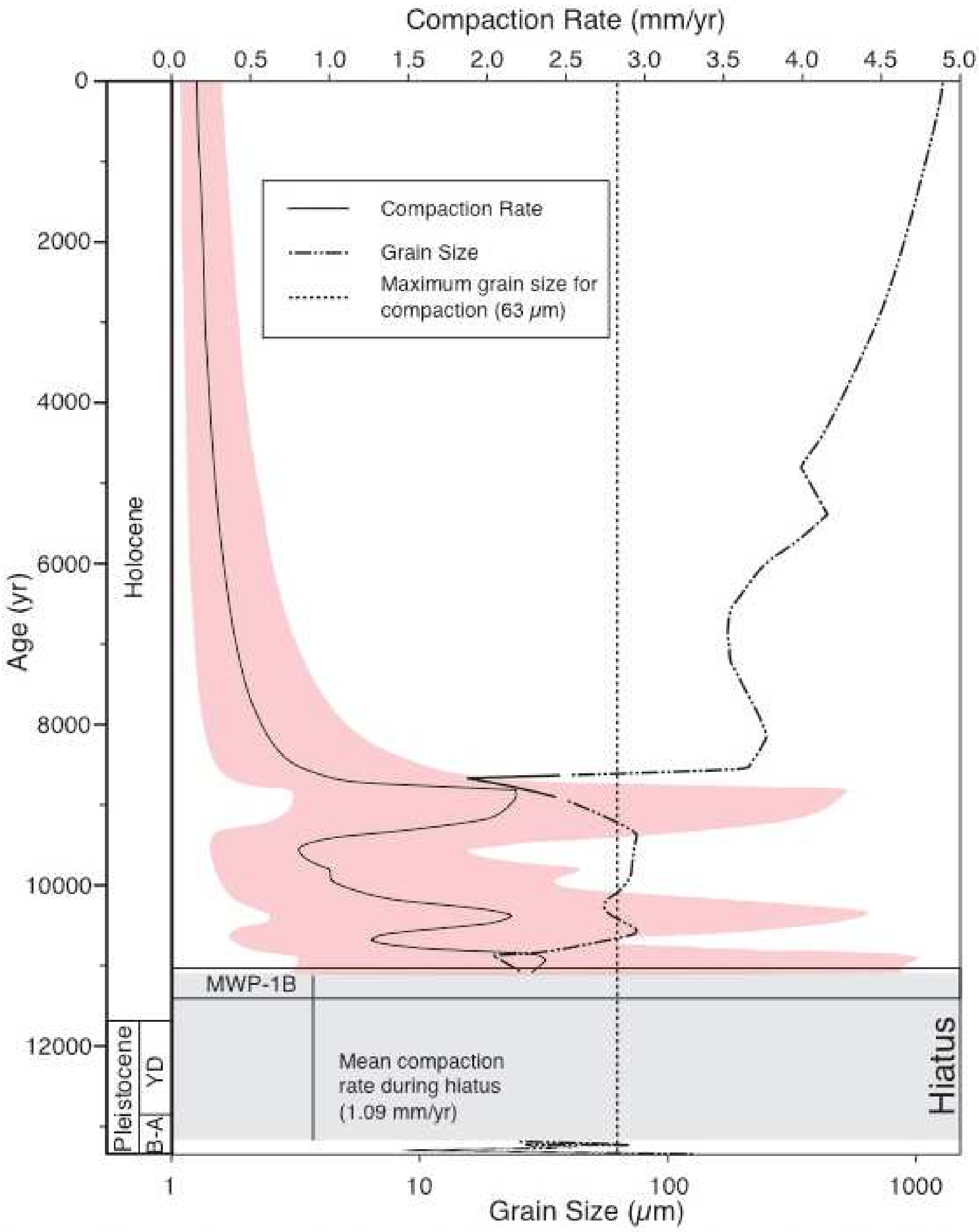

Fig. 7: Modeled compaction rate at NMY through time, calculated using a porosity model (Equation 1) that is a function of median grain size, burial depth, and age at the NMY through time (solid red line) with 2σ error (red shaded area). Compaction rate at any given time is strongly influenced by the grain size of the sediments being deposited at that time (intermittent dashed line). Sediments with grain size above 63 µm (vertical dashed line) were assumed to be

incompressible. B-A = Bølling-Allerød; YD = Younger Dryas. Dates for events and time periods are from Rasmussen et al., 2006, Deschamps et al., 2012, and Abdul et al., 2016.

underlying layer. In this way, each layer is able to respond to the removal of the top layer and thickness changes in each layer remaining above it. Because sands and larger particles are assumed to be relatively incompressible on the time scales and depths found in the NMY section, the model did not calculate porosity changes for sediments >63 µm (illustrated by the vertical line in Fig. 7). This layer-by-layer method makes it possible to see how the rate of compaction varies through time and provides a more realistic estimate of the modern contribution of compaction to the relative rate of sea-level rise at the Sandy Hook tide gauge. The model scripts are available in the supplementary material.

4.0 Results

4.1 Drilling Results

The cores were drilled to 86.9, 77.7, and 53.3 m at the NMY, SS, and SMY-A sites respectively (Figs. 4, 5, S1, and S2). At the NMY, adjacent to the tide gauge, we recovered 84+ m of Quaternary sands and silts overlying the inferred Quaternary/Cretaceous contact. At the base, there was a thin (3+ m) layer of upper Pleistocene basal gravels interpreted as a post-glacial fluvial deposit (Figs, 3, 4; Stanford et al., 2015; Miller et al., in press) overlain by thick (25 m) moderately organic-rich (up to 1.9%) sandy clayey silts. These sediments are a mix of thinly laminated planar, cross-laminated, and massive layers and were deposited in deltaic/estuarine environments (Figs, 3, 4; Stanford et al., 2015; Miller et al., in press). This unit is separated from the overlying strata by a surface at 55.1 m marked by sediment disturbance and possibly erosion. The surface is overlain by 13 m of lower Holocene silty sands and sandy silts. At ~43.7 m, benthic foraminiferal (*Elphidium*, *Guttulina)*, diatoms, and sponge spicules have all been identified leading to the interpretation that these sediments were deposited in estuarine environments (Stanford et al., 2015; Miller et al., in press). Above these silty sands are 20 m of middle Holocene medium to well-sorted sands containing frequent large wood fragments, lignite, and lithic fragments suggesting a strong riverine influence, supporting the interpretation of an estuarine deposit (Miller et al., in press). Thick (18 m) upper Holocene gravelly sands overlie these sands. The coarse nature of the sediments indicates a higher energy environment supporting an upper shoreface interpretation for the environment of deposition (Stanford et al., 2015; Miller et al., in press). The uppermost 5 m consists of moderately well-sorted medium to coarse sands (past 1000 years, Fig. 6) deposited contiguous with the modern prograding shoreface. Recovery was very poor in the uppermost ~24 m.

A similar succession of sediments occurs at the SS (Fig. 5) with the Cretaceous/Quaternary contact at 59.2 m. Here, more competent compacted glauconite silts of the Merchantville Formation and silty clays of the overlying Woodbury Formation are overlain by ~4 m of unconsolidated uppermost Pleistocene sands and gravels interpreted as a glaciofluvial deposit covered by 16.5 m of alternating laminated and massive silts deposited in estuarine environments (Stanford et al., 2015; Miller et al., in press). Above this are 8.2 m of Holocene medium to fine silty sands. This unit is overlain by 11.5 m of slightly clayey gravelly sands deposited in tidal channel or estuarine environments (Stanford et al., 2015; Miller et al., in press). The uppermost 23 m consists of gravelly sands with some gravel concentrated into distinct layers representing deposition in shoreface environments contiguous with the modern spit. Recovery was limited though this interval.

At the SMY-A (Fig. S2), the Quaternary/Cretaceous contact was at 47.1 m. It is overlain by 1.9 m of glaciofluvial gravel. The gravel is overlain by 22.2 m of slightly silty sands that are in turn overlain by 3.7 m of slightly silty fine sand deposited in estuarine environments overlain by 19.3 m of slightly silty medium to coarse sand deposited in tidal channel and shoreface environments.

4.2 Grain Sizes

Grain sizes across all three cores generally fine upward in the lower section of Quaternary sediments and coarsen upward in the upper section (Table ST5). At the NMY (Fig. 4), sediments generally fine upward from 84 to 72.5 m, with median grain sizes transitioning from gravels at the base to ~8 µm fine silt. Above 72.5 m, the sediments coarsen upward to ~70 µm (median grain size) at 63.5 m. Grain sizes then decrease to ~20 µm silts at 54.5 m. Above 54.5 m, the sediments coarsen upward to coarse sand (1.2 mm) and gravels in the uppermost 20 m. There is a fine grained (~15 µm) bed at 43.3 m. The SS (Fig. 5) shows similar trends in the Quaternary section with a coarse basal section of ~300 µm sands fining upward to ~7 µm at 45 m. The section then coarsens to coarse sands (~600 µm) and gravels around 33 m. The uppermost 30 m at the SS is composed primarily of medium (350-400 µm) sands. The entire Quaternary section at the SMY-A (Fig. S2) consists of medium sands with median values between 250 and 450 µm, with a thin interval of coarse silts and fine sands (48-141 µm) from 19.2-23 m.

4.3 Percent Organic Matter

Organic matter content in the Quaternary sections (Figs. 4-5, S2, Table ST6) is low, with values of ~0.4-1.5% and an average of ~1% for most sands and ~1-6% with an average of ~4% in the silts. As grain size decreases, the %OM typically increases. Aside from thin (< ~1 mm) laminae, the organic material is typically suspended in a siliciclastic matrix. At the NMY, %OM decreases upsection from peak values of ~5% in the upper Pleistocene and lower Holocene silts. The %OM reaches 1.2-1.9% between 53-43 m before decreasing to values of ~0.9-0.2% in the uppermost 43 m. At the SS site, the basal Quaternary section from 59.21 to 54.40 m consists of between 0.6 and 1.7 % OM. Above 54.40 m, the %OM increases to 4.9% at 48.31 m before decreasing to 0.5 % at 32.46 m. The uppermost 32.46 m have %OM values generally ≤0.5% with intervals of 1.3 and 2.2 % at 34.56 and 11.12 m, respectively. Similar to grain size, the SMY-A shows much less variability with samples throughout the section generally containing between 0.3 and 0.5 % organic carbon.

4.4 Radiocarbon Ages and Age Models

Radiocarbon age estimates (Table 1) indicate high mean sedimentation rates of 400-500 cm/kyr during the Holocene (Fig. 6). At the base of the NMY there are 30 m of sediment with 5 radiocarbon ages that range from 13,350-13,150 cal yrs BP. The best estimate is that these silts were deposited in < 200 years with a mean sedimentation rate of 15,000 cm/kyr and are associated with the Lake Iroquois outburst floods (Rayburn et al., 2005; Donnelly et al., 2005; Thieler et al., 2007). We interpret the previously described surface at 55.1 m, directly above these rapidly emplaced sediments to be an unconformity. Based on our age model, this surface represents a hiatus from 13,150-11,060 cal yrs BP. Above the unconformity, the sedimentation rate decreases to 500 cm/kyr.

At the SS, there is a similar section of sediments at the base of the Quaternary with radiocarbon ages between 13,300 and 13,000 cal yrs BP, that we interpret to be the same time interval represented by the 30 m package of sediments at the base of the NMY. This results in a mean sedimentation rate of 7,200 cm/kyr. Above this unit, while there is no obvious surface visible in the lithology as seen at the NMY, we infer an unconformity at 44.8 m, which, based on our age model, marks a hiatus from 13,150 to 12,130 cal yrs. This is supported by the rapid shift in mean sedimentation rates from 7,200 cm/kyr below to 200 cm/kyr from 39.3 to 44.8 m and then 420 cm/kyr in the uppermost 39.3 m. Whereas age resolution increases with depth at the NMY and SS, poor organic preservation limits age control on the SMY-A core precluding any further analysis.

4.5 Porosity

At the NMY site, porosity generally tracks grain size (Fig. 4, Table ST7) increasing from 31.2% at the base to between 50 and 60% from 83.37 to 60.55 m. Porosity decreases to between 34.9 and 38.6% from 60.55 to 34.61 m before increasing to 44.6% at 33.09 m. Values then decrease to 20.2% by 1.75 m.

At the SS site (Fig. 5), porosities are generally lower with a basal porosity of 41.9% at 58.79 m in the upper Pleistocene. Values then increase to 59.0% at 54.05 m before decreasing to 45.9% at 51.37 m. Porosity then increases to 55.1% at 45.27 m, then porosity decreases to between ~20 and ~30% for the uppermost 45.27 m.

Porosities at the SMY-A (Fig. S2) show little variability with values between 46.5 and 31.1% for the entire section. There are no strong trends, rather the porosity seems fairly steady between 36 and 38% with several excursions.

The error associated with the porosity measurements is generally low ≤4%. Error increases with grain size. In coarser samples (>63 µm median grain size) the average error (1??) is ~4% with a maximum of ~8% in some of the coarsest samples. For finer samples (<63µm) the average error (1??) is closer to 1%. The error is sampled in the numerical model to define the error in the model results.

5.0 Discussion

Local processes must be invoked to explain the 0.9±0.5 mm/yr additional, non-GIA-related RSL rise at Sandy Hook relative to The Battery. The potential contributors to the locally high relative rate of sea-level rise include compaction of organic material or peats, compaction of inorganic silts and clays, and anthropogenic compaction resulting from groundwater removal. This study revealed that compaction of Quaternary silts and clays and groundwater removal are the two primary factors controlling the localized sea-level change at Sandy Hook. While organic material has a negligible impact on the rate of RSL rise at Sandy Hook, compaction of inorganic Quaternary sediments is a contributor, and there is evidence that groundwater extraction may also be a key factor.

5.1 Depositional Environments

The majority of the non-anthropogenic compaction at Sandy Hook is derived from the relatively young (<13,350 cal yr BP) sediments (Fig. 3). We base the following history primarily upon results from the NMY site, though the general trends are similar at the SS site. The Quaternary sediments lie above an unconformity separating Cretaceous and uppermost Pleistocene strata. The most striking feature of the sedimentary record under Sandy Hook is the thin (+3 m) layer of gravels. Above the gravels there is ~25 m of sediment deposited rapidly between 13,350-13,150 cal yrs BP. The thick, rapidly deposited sediment unit drives the compaction (Fig. 7) and our interpretation of the deglacial history. Based on the radiocarbon evidence from the overlying 25 m of silts, and the timing of the incision of the Raritan and Hudson shelf valleys, which border Sandy Hook (Stanford, 2010), we interpret the 3+ m of basal gravels to be post-glacial fluvial deposits. The ~25 m of overlying postglacial silts (Qmm^2, Fig. 3) were then deposited rapidly (13,350-13,150 cal yrs BP). Given the close match of radiocarbon ages, we suggest that the silts are the result of multiple floods that discharged from Glacial Lake Iroquois and down the Hudson Valley at that time (Rayburn et al., 2005; Donnelly et al., 2005; Thieler et al., 2007). Based on the presence of occasional cross laminations and wavy bedding, the sediments were deposited in an estuarine or deltaic environment. As the sediment saturated waters of the Hudson River reached the mid to lower estuarine environment near modern day Sandy Hook, there was likely rapid deposition as seen in the modern Hudson Estuary (Traykovski et al., 2004). Above these postglacial silts, is an unconformity that, based on our age model, marks a hiatus from 13,150-11,060 cal yrs. Overlying the unconformity are 13 m (11,060-8,600 cal yrs) of mid-estuarine silty sands. Above this, 20 m (8,600-4,600 cal yrs) of estuarine sediments coarsen upward from silty sands to sands. This unit is overlain by 18 m (4,600-1,000 cal yrs) of sands interpreted to be shoreface and channel sands. The uppermost 5 m is composed of coarse sand deposits of the modern (1,000 cal yr BP-present) barrier island.

5.2 Minimal Organic Compaction

Previous studies of organic-rich Quaternary nearshore deposits in England and the U.S. Gulf of Mexico (Horton and Shennan, 2009; Törnqvist et al., 2008) have shown that compaction of organic rich layers could make a significant contribution to local subsidence. During and after drilling, the cores were examined for thick peats, deposits that could contribute significantly to the subsidence at Sandy Hook. While there are thin, millimeter thick organic-rich laminae, there are no evident organic zones and the OM values are relatively low (< 2%). The error on the measurements (<3%) is negligible (see supplement for uncertainty estimation). Even at the high end of the error at the NMY, there is insufficient organic material for the sediments to be classified as carbonaceous. Furthermore, the dispersed nature of the organics and lack of thick, concentrated bands of peats suggest that the compaction of the organic material would be dependent on the compaction of the siliciclastic matrix. The %OM values measured in this study (0.4-1.9%), are within the range measured in modern estuaries (~1-10%; Thornton and McManus, 1994; Andrews et al., 1998). This suggests that the organic material is not undergoing decomposition. Based on this, we conclude that there is insufficient organic material present and it is not concentrated enough to be a significant contributor to the subsidence at Sandy Hook.

5.3 Siliciclastic Compaction

Compaction of siliciclastic sediment is another potential contributor to Sandy Hook's subsidence history. Sandy Hook, particularly near the tide gauge, is underlain by a thick (85+ m) Quaternary section, the lower ~40 m of which is dominantly silts with the potential to compact nearly 50% due to porosity loss through time and burial (Kominz et al., 2011).

Our regression models indicate that the rate at which a unit of silt compacts decays exponentially through time as the unit approaches its minimum porosity (~40% based on the Cretaceous section at the SS site). Without the addition of new silts, the rate of compaction in the entire sediment column would eventually reach ~0 mm/yr. Note that this has been the case at the NMY since ~8,500 cal yr BP, when the deposition of mud ceased; our forward model indicates that the rate of compaction has decayed since this time to the modern rate (Fig. 7). Due to the thick Quaternary section, the numerical model of porosity as a function of grain size, burial depth, and age (Equation 1) yields an average 20th century compaction rate of 0.16 mm/yr (90% C.I. 0.06-0.32) that can be attributed to the natural compaction of the siliciclastic sediments underlying the northern portion of Sandy Hook. When porosity is modeled only as a function of grain size and burial depth (Equation 2), the rate is 0.19 mm/yr (90% C.I. 0.03-0.39; Fig. S7). Based on the lower AIC and higher r^2 values of Equation 1 indicate that the Equation 1 model is preferred. The 90% C.I. of 0.06 to 0.32 mm/yr from Equation 1 ranges from nearly zero impact to ~1/3 of the local rate of sea-level rise at Sandy Hook. When the rate of compaction is subtracted from the local rate of sea-level rise, the remaining rate is 0.7 mm/yr (90% C.I. 0.3-1.2). This suggests that there is still a significant source of local sea-level rise that is unaccounted for.

During deposition following the glacial outburst, rates of compaction were on the order of 10s of mm/yr, peaking between ~40 and ~80 mm/yr. Compaction during this period was high due to rapid (15,000 cm/kyr) deposition supplying a large amount of highly compressible silts (Fig. 7). In addition to supplying silts, the high sedimentation rate also means that the sediments were rapidly buried. The rate is further augmented by the ability of deposited silts to quickly lose porosity after deposition (Woodruff et al., 2001).

The modeled rates of compaction include natural compaction and compaction due to groundwater pumping from the Quaternary units we sampled. Historical records show that groundwater extraction from the Quaternary sediments at Sandy Hook began in the 1890's. Any drawdown in the groundwater levels resulting from that pumping would have induced compaction and affect our porosity measurements. However, our model shows that the majority of natural compaction occurred during the early Holocene and has decayed exponentially to present (Fig. 7). This concentrates any model uncertainty due to porosity uncertainties in the early portion of the record, resulting in a minimal influence on the modeled 20th century rate. Also, most groundwater pumping effects would be expected from the much more heavily pumped Cretaceous aquifers (see Section 5.4 below). While groundwater effects may influence the modeled ~0.16 mm/yr Quaternary compaction, the dominant effect controlling the modeled 20th century compaction rate is the compaction of the deglacial silts (Fig. 7).

Poor recovery in the uppermost ~24 m at the NMY adds some uncertainty to the numerical model, particularly in the recent portion of the model. However, poor recovery is associated with coarse sands as indicated by the gamma log (Fig. 4), less cohesive sediments that would be excluded from the model. Also, the log signatures in the unrecovered intervals indicate coarse sediments and shows that there are no significant lithologic changes that would have been missed in the unrecovered intervals, lending additional support that the unrecovered intervals likely had a negligible impact on the rate of compaction at Sandy Hook.

5.4 Groundwater Withdrawal

With a 20th century natural compaction rate of 0.16 mm/yr (90% C.I. 0.06-0.32) for siliciclastic sediments, there is 0.7 mm/yr (90% C.I. 0.3-1.2 mm/yr) of subsidence at Sandy Hook that is unaccounted for. We hypothesize that groundwater withdrawal is potentially a leading cause of this subsidence, making it the dominant local contributor after GIA. Land subsidence due to groundwater pumping in confined aquifers is a well-documented phenomenon of the 20th century (see review in Galloway et al. 1999; Sun et al., 1999; Galloway and Burby, 2011; Galloway and Sneed, 2013). Pertaining to Sandy Hook, historical records of local groundwater depletion and previous regional groundwater models support this hypothesis, suggesting significant drawdown of the groundwater level underlying Sandy Hook (dePaul et al., 2008).

Regarding local effects, the Sandy Hook tide gauge is located ~2 km from the Ft. Hancock Pumping Station, adjacent to the SS site (Fig. 1). The pumping station is the sole water source for facilities located on Sandy Hook. It has also been the site of many wells servicing Fort Hancock over the years. Construction of Fort Hancock began in 1896 at which time 36 artesian wells were installed to supply 150,000 gallons of water per day (Bearss, 1981). During installation of one well point, the drillers encountered a pocket of pressurized gas at ~45 m (~151 ft) that they described as carbonic acid. The resulting ~15 m (50 ft) geyser of sand and water lasted for more than 5 hours. Once the artesian wells were established, they began to show signs of depletion by 1905 and most were exhausted by 1907 (Bearss, 1981). This evidence shows that even before the base reached its largest population during World War II (Fig. 8), Fort Hancock caused a significant drawdown of the local groundwater level.

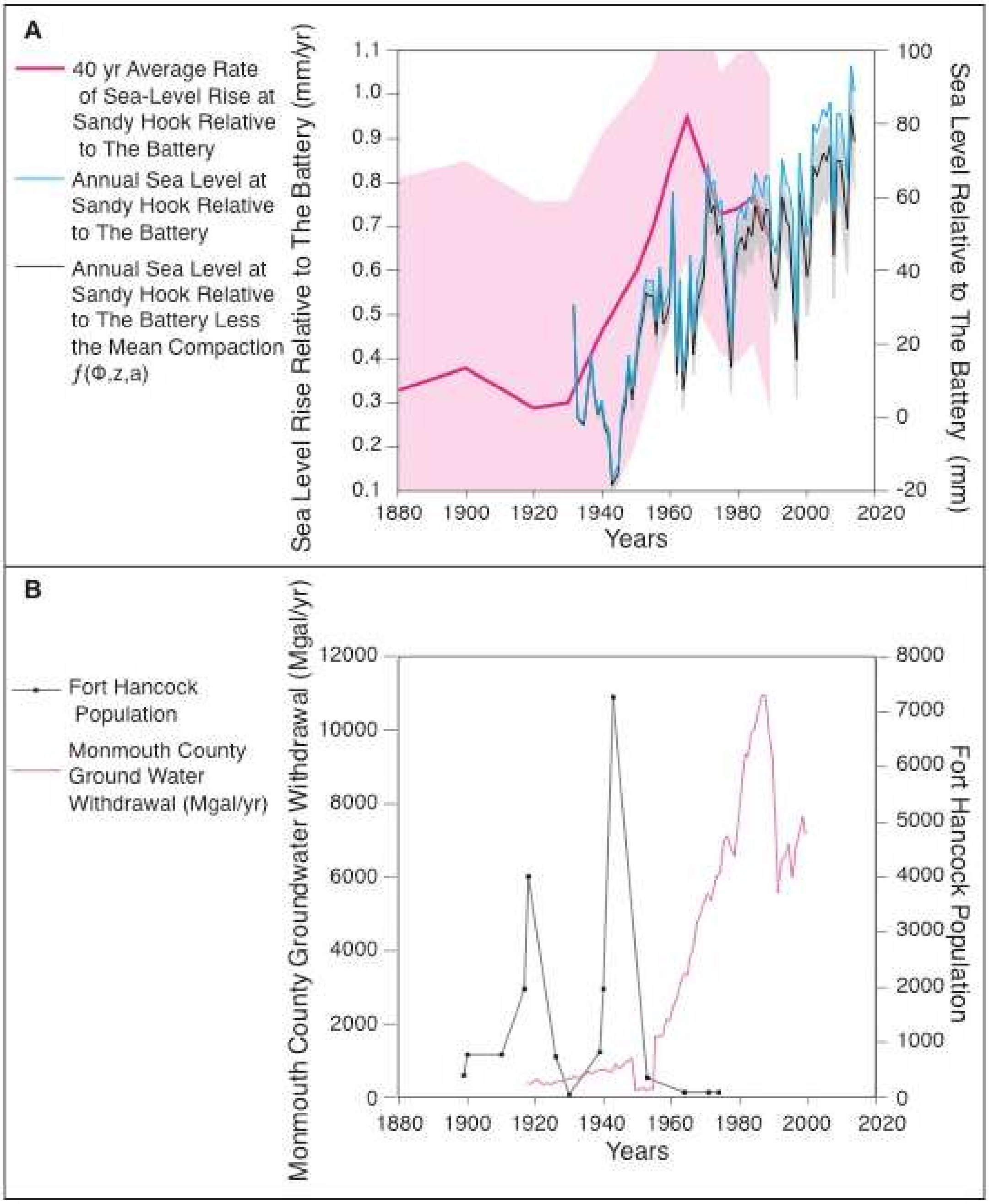

Fig. 8: Sea Level vs. Groundwater Withdrawal. A: Modeled 40 yr average rate of sea-level rise at Sandy Hook minus the rate at The Battery with 2σ uncertainty (pink; see supplementary section S1.9 for method), Annual sea level at Sandy Hook minus The Battery (cyan) and the sea level at Sandy Hook minus The Battery and modeled compaction with 2σ uncertainty (black). B: The rate of regional groundwater withdrawal for Monmouth County (magenta) and the local

population of Ft. Hancock (black), a proxy for groundwater withdrawal (Bearss, 1981; T. Hoffman personal communication; Hoffman, T., An Old Army Town; Holgate et al., 2013; Permanent Service for Mean Sea Level, 2016; J. Shourds, personal communication).

The population of Fort Hancock, a proxy for the local groundwater withdrawal, is shown with the regional groundwater pumpage from Monmouth County southwest of Sandy Hook (Fig. 8). From the onset of significant withdrawal on the mainland in the early 20th century to 1980 aquifers underlying the northern portion of Sandy Hook experienced a cumulative ~9-18 m (30-60 ft) decrease in water level (Fig. 9) (dePaul et al., 2008).

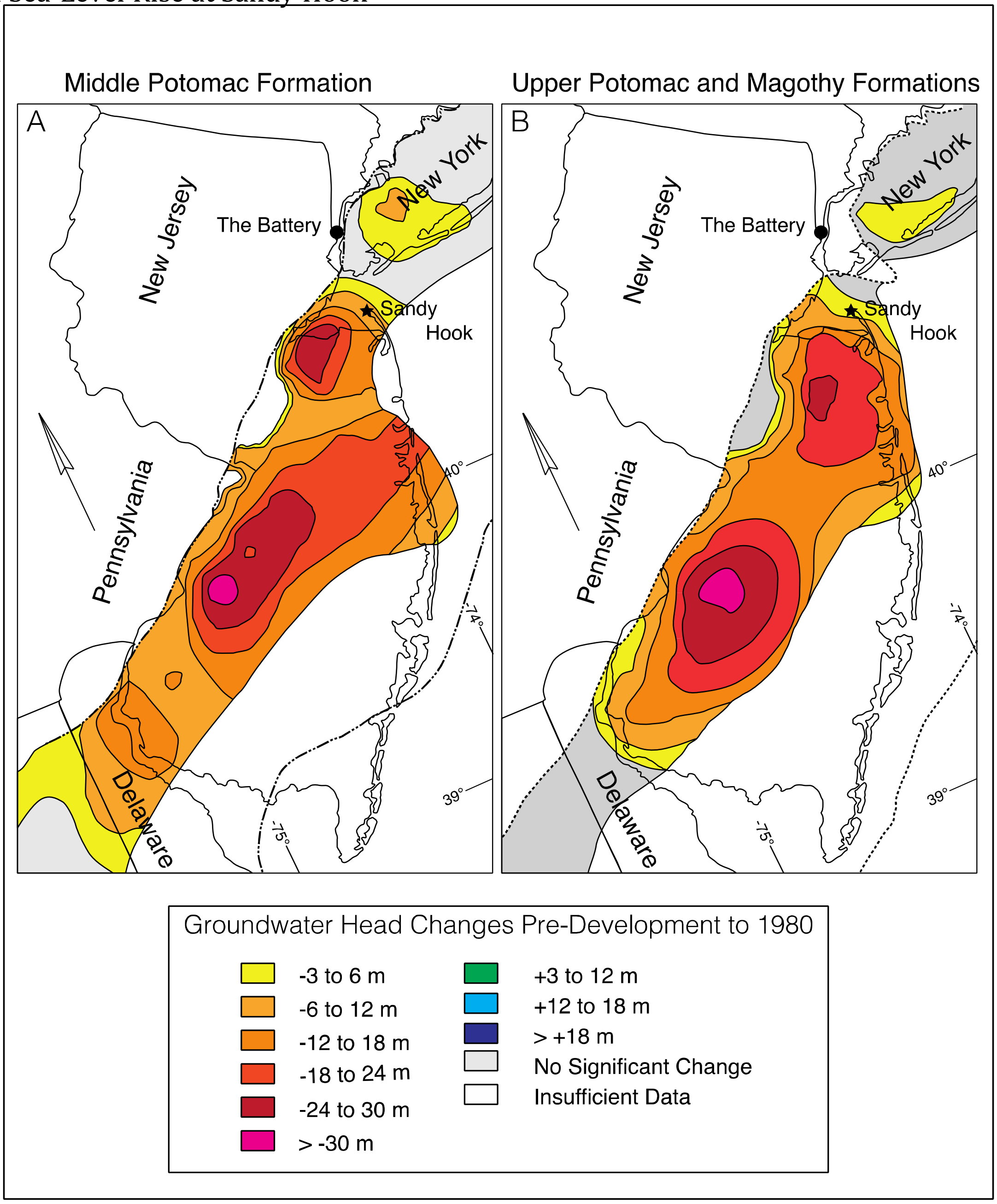

Fig. 9: Estimated groundwater level changes pre-development to 1980. A: The Middle Potomac Formation, B: The Upper Potomac and Magothy Formations. Modified from dePaul et al. (2008).

The period between 1980-2000 saw no significant change in the water levels in the underlying aquifers, because withdrawals were curtailed beginning in 1990 to prevent saltwater intrusion (dePaul et al., 2008). The overlapping local and regional drawdowns are likely sufficient to reduce pore fluid pressure in the underlying strata, thereby allowing compaction and subsidence (Holzer and Galloway, 2005). While there does appear to be a link between the timing of changes in the local rate of RSL rise at Sandy Hook and the events in the history of groundwater withdrawal (Fig. 8), it is not straightforward. The disconnect may be due to a lag between the drawdown of groundwater and the compaction of fine grained sediments in the confining units above and below the aquifers as documented by Sneed and Galloway (2000). Furthermore, the 40 year average for the rate of sea-level rise at Sandy Hook relative to the Battery (Fig. 8A) also introduces a lag. Future groundwater modeling will attempt to test this hypothesis and provide insight into the relative contributions of local and regional groundwater withdrawal to the subsidence at Sandy Hook.

Our quantification of contributions from global mean, regional (especially GIA), and local (compaction due to natural and anthropogenic change) effects can be applied to other regions using the principles and compaction model developed here. Whereas the greatest uncertainty in planning for regional and local projections is the global response of thermal expansion and continental ice sheets (Kopp et al., 2014, 2017), we show that not only can we quantify the regional GIA response (Kopp, 2013; Miller et al., 2013; Kopp et al., 2016), we can also quantify contributions from natural compaction and attribute the remainder to compaction induced by groundwater withdrawal. For example, our approach can be applied used to make predictions for the entire Mid-Atlantic U.S. region based on the local Quaternary geology and local/regional groundwater withdrawal rates. By considering cones of depression (e.g., Fig. 9; DePaul et al., 2008) and considering groundwater extraction rates, we predict that lower rates of local subsidence would be experienced from Cape May, NJ south through much of the Delmarva peninsula.

6.0 Conclusion

After accounting for GIA, tide gauge records from Sandy Hook, NJ and The Battery, NY, show a 0.9±0.5 mm/yr difference in the 20th century rates of sea-level rise experienced at two locations within 26 km of each other. Based on the low organic matter in our corehole transect, we eliminate compaction of organic material as a significant contributor at Sandy Hook. Based on our porosity, grain size, and age constraints, we model natural subsidence due to compaction as 0.16 mm/yr (90% C.I. 0.06-0.32 mm/yr). The remaining 0.7 mm/yr (90% C.I. 0.3-1.2 mm/yr) is likely due to anthropogenic groundwater withdrawal. Future work will attempt to constrain the relative contributions of both regional and local groundwater withdrawal to Sandy Hook's subsidence history.

7.0 Acknowledgements

We thank G. Ashley for numerous insightful discussions and the use of her lab for sample processing, I. Hong and T. Dura for their help and instruction when running the Malvern Mastersizer 3000, C. Fuller and G. Taghon at the Benthic Ecology Lab for their assistance with LOI measurements, M. Kominz for insights into modeling decompaction and changes in porosity, J. Shourds at the U.S. Geological Survey for enlightening insights and information on groundwater usage in the New Jersey Coastal Plain, A. Fiore at the U.S. Geological Survey for insightful discussions and information on historical wells at Ft. Hancock, and T. Hoffman at the National Park Service for help when researching historic groundwater extraction and base population at Ft. Hancock. We would like to acknowledge three anonymous reviewers and the editorial oversight of I. Hendy whose contributions helped to improve the paper. Drilling was supported by the New Jersey Geological and Water Survey and NSF Grants OCE14-63759 and OCE-1154379 (Miller). This publication is the result of research sponsored by the New Jersey

Sea Grant Consortium (NJSGC) with funds from the National Oceanographic and Atmospheric Administration (NOAA) Office of Sea Grant, U.S. Department of Commerce, under NOAA grant number NA14OAR4170085. It was also supported by the Nation Science Foundation (OCE-1458904 to Horton and Kopp). The statements, findings, conclusions, and recommendations are those of the authors and do not necessarily reflect the views of the funding agencies. NJSGC Publication Number: NJSG-17-927 and Earth Observatory of Singapore Contribution 171.

7.0 References

Abdul, N.A., Mortlock, R.A., Wright, J.D., and Fairbanks, R.G., 2016. Younger Dryas sea level and meltwater pulse 1B recorded in Barbados reef crest coral *Acropora palmata*. Paleoceanography, v. 31, is. 2, p. 330-344.

Andrews, J.E., Greenaway, A.M., and Dennis, P.F., 1998. Combined carbon isotope and C/N ratios as indicators of source and fate of organic matter in a poorly flushed tropical estuary: Hunts Bay, Kingston Harbor, Jamaica. Estuarine, Coastal and Shelf Science, v. 46, n. 5, p. 743-756.

Bearss, E.C., 1981. Historic resource study Fort Hancock 1895-1948: Gateway National Recreation Center New York/New Jersey. National Park Service, Denver, Colorado.

Blaauw, M., Christen, J.A., 2011. Flexible paleoclimate age-depth models using an autoregressive gamma process. Bayesian Analysis, v. 6, p. 457-474.

Brian, M.J., Kemp, A.C., Horton, B.P., Culver, S.J., Parnell, A.C., Cahill, N., 2015. Quantifying the contribution of sediment compaction to late Holocene salt-marsh sea-level reconstructions, North Carolina, USA. Quaternary Research, v. 83, n. 1, p. 41-51.

Chen, X., Zhang, X., Church, J.A., Watson, C.S., King, M.A., Monselesan, D., Legresy, B., and Harig, C., 2017. The increasing rate of global mean sea-level rise during 1993-2014. Nature Climate Change, v. 7, n. 7, p. 492-495.

Church, J.A., and White., N.J., 2011. Sea-level rise from the late 19th to the early 21st century. Surveys in Geophysics, v. 32, n.4-5, p. 585-602.

Clark J.A., Farrell, W.E., and Peltier, W.R., 1978. Global changes in postglacial sea level: A numerical calculation. Quaternary Research, v. 9, p. 265-287.

Cronin, T.M., 2012. Rapid sea-level rise. Quaternary Science Reviews, v. 56, p. 11-30.

Dangendorf, S., Marco, M., Wöppelmann, G., Conrad, C. P., Frederikse, T., and Riva, R., 2017. Reassessment of 20th century global mean sea level rise. PNAS. v. 114, n. 23, p. 5946-5951.

dePaul, V.T., Rice, D.E., and Zapecza, O.S., 2008. Water-level changes in aquifers of the Atlantic Coastal Plain, predevelopment to 2000. U.S. Geological Survey Scientific Investigations Report 2007-5247, p 1-88.

Deschamps, P., Durand, N., Bard, E., Hamelin, B., Camoin, G., Thomas, A.L., Henderson, G.M., Okuno, J., and Yokoyama, Y., 2012. Ice-sheet collapse and sea-level rise at the Bølling warming 14,600 years ago. Nature, v. 483, p. 559-564.

Donnelly, J.P., Driscoll, N.W., Uchupi, E., Keigwin, L.D., Schwab, W.C., Thieler, E.R., and Swift, S.A., 2005. Catastrophic meltwater discharge down the Hudson Valley: a potential trigger for the Intra-Allerød cold period. Geology, v. 33, no. 2, p. 89-92.

Galloway D., D.R. Jones, and S.E. Ingebritsen, 1999. Land Subsidence in the United States. U.S. Geological Survey Circular 1182. https://pubs.usgs.gov/circ/circ1182/

Galloway D., and J. Burbey, 2011. Review: Regional land subsidence accompanying groundwater extraction. Hydrogeology Journal. v.19, p. 1459–1486.

Galloway D., and M. Sneed, 2013. Analysis and simulation of regional subsidence accompanying groundwater abstraction and compaction of susceptible aquifer systems in the USA. Boletín de la Sociedad Geológica Mexicana. v. 65, n. 1, p. 123-136.

Gurnis, M., 1990. Bounds on global dynamic topography from Phanerozoic flooding of continental platforms. Nature, v. 344, p. 754-756.

Hay, C.C., Morrow, E., Kopp, R.E., and Mitrovica, J.X., 2015. Probabilistic reanalysis of twentieth-century sea-level rise. Nature, v. 517, p. 481-484.

Heiri, O., Lotter A.F., and Lemcke, G., 2001. Loss on ignition as a method for estimating organic and carbonate content in sediments: reproducibility and comparability of results. Journal of Paleolimnology, v. 25, p. 101-110.

Hoffman, T.J.. An old army town. https://www.nps.gov/gate/learn/historyculture/upload/old_army_town.pdf [17 May, 2016]

Holgate, S.J., Matthes, A., Woodworth, P.L., Rickards, L.J., Tamisiea, M.E., Bradshaw, E., Foden, P.R., Gordon, K.M., Juvrejeva, S., Pugh, J., 2013. New data systems and products at the permanent service for mean sea level. Journal of Coastal Research, v. 29, n. 3, p. 493-504.

Holzer, T.L. and Galloway, D.L., 2005. Impacts of land subsidence caused by withdrawal of underground fluids in the United States. in Ehlen, J., Haneberg, W.C., and Larson, R.A., eds., Humans as Geologic Agents: Boulder, Colorado, Geological Society of America Reviews in Engineering Geology, *16*, 87-99. doi:10.1130/2005.4016(08)

Horton, B.P., and Shennan, I., 2009. Compaction of Holocene strata and the implications for relative sea-level change on the east coast of England. Geology, v. 37, n. 12, p. 1083-1086.

Jevrejeva, S., Moore, J.C., Grinsted, A., and Woodworth, P.L., 2008. Recent global sea level acceleration started over 200 years ago? Geophysical Research Letters, v. 35, n. 8.

Kemp, A.C., Horton, B.P., Donnelly, J.P., Mann, M.E., Vermeer, Martin, and Rahmstorf, S., 2011. Climate related sea-level variations over the past two millennia. Proceedings of the National Academy of Sciences, v. 108, n. 27, p. 11017-11022.

Kominz, M.A., Browning, J.V., Miller, K.G., Sugarman, P. J., Mizintseva, S., and Scotese, C.R., 2008. Late Cretaceous to Miocene sea-level estimates from the New Jersey and Delaware coastal plain coreholes: An error analysis. Basin Research, v. 20, n. 2, p. 211-226.

Kominz, M. A., Paterson, K., and Odette, D., 2011. Lithology dependence of porosity in slope and deep marine sediments. Journal of Sedimentary Research, v. 81, p. 730-742.

Kopp, R.E., 2013. Does the mid-Atlantic United States sea-level acceleration hot spot reflect ocean dynamic variability? Geophysical Research Letters, v. 40, p. 3981-3985.

Kopp, R.E., Hay, C.C., Little, C.M., and Mitrovica, J.X., 2015. Geographic variability of sea-level change. Current Climate Change Reports, v. 1, p. 192-204.

Kopp R.E., Kemp, A.C., Bittermann, K., Horton, B.P., Donnelly, J.P., Gehrels, W.R., Hay, C.C., Mitrovica, J.X., Morrow, E.D., and Rahmstorf, 2016. Temperature-driven global sea-level variability in the common era. Proceedings of the National Academy of Sciences, v. 113, n. 11, E1434-E1441.

Kopp, R.E., Deconto, R.M., Bader, D.A., Horton, R.M., Hay, C.C., Kulp, S., Oppenheimer, M., Pllard, D., and Strauss, B.H., 2017. Implications of Antarctic ice-cliff collapse and ice-shelf hydrofracturing mechanisms for sea-level projections. ArXiv e-prints. eprint: 1704.05597.

Lyttle, P.T., and Epstein, J.B., 1987. Geologic map of the Newark 1°x2° quadrangle, New Jersey, Pennsylvania, and New York. U.S. Geological Survey, Miscellaneous Investigations Series 1-1715.

McNeely R., Dyke A. S., and Southon J. R., 2006. Canadian marine reservoir ages, preliminary data assessment, Open File 5049, pp. 3. Geological Survey Canada.

Miller K.G., Kopp, R.E., Horton, B.P., Browning, J.V., and Kemp, A.C., 2013. A geological perspective on sea-level rise and its impacts along the U.S. Mid-Atlantic Coast. Earth's Future, v. 1, n. 1, p. 3-18.

Miller, K.G., Sugarman, P.J., Stanford, S., Browning, J.V., Baldwin, K., Buttari, B., Dunham, B., Farazaneh, M., Filo, R., Gagliano, M.P., Horton, B., Gallegos, G., Graham, S., Johnson, C., Khan, N., Kulhanek, D.K., Lombardi, C.J., McKoy, K., McLaughlin, P.P., Monteverde, Jr., D.H., Stanley, J.N., Woodard, S., and Malerba, N., in press. Sandy Hook site report, in Miller, K.G., Sugarman, P.J., Browning, J.V., et al., eds., Proceedings of the Ocean Drilling Program, Initial reports, Volume 174AX (Suppl.): College Station, TX, Ocean Drilling Program.

Minard, J. P., 1969. Geology of the Sandy Hook quadrangle in Monmouth County, New Jersey. U. S. Geological Survey Bulletin 1276, p. 43.

Moucha, R., Forte, A.M., Mitrovica, J.X., Rowley, D.B., Quéré, S., Simmons, N.A., and Grand, S.P., 2008. Dynamic topography and long-term sea-level variations: There is no such thing as a stable continental platform. Earth and Planetary Science Letters, v. 271, n. 1, p. 101-108.

Owens, J.P., Sugarman, P.J., Sohl, N.F., Parker, R.A., Houghton, H.F., Volkert, R.A., Drake, A.A., and Orndorff, R.C., 1998. Geologic map of Central and Southern New Jersey. U.S. Geological Survey, Miscellaneous Investigation Series Map I-2540-B.

Permanent Service for Mean Sea Level (PSMSL), 2016. Tide Gauge Data. http://www.psmsl.org/obtaining/ [17 July, 2016]

Pope, J.P., and Burbey, T.J., 2004. Multiple-aquifer characterization from single borehole extensometer records. Ground Water, v. 42, n. 1, p. 45-54.

Rasmussen, S.O., Andersen, K.K., Svensson, A.M., Steffensen, J.P., Vinther, B.M., Clausen, H.B., Siggard-Andersen, M.-L., Johnson, S.J., Larsen, L.B., Dahl-Jensen, D., Bigler, M., Röthlisberger, R., Fischer, H., Goto-Azuma, K., Hansson, M.E., and Ruth, U., 2006. A new Greenland ice core chronology for the last glacial termination. Journal of Geophysical Research, v. 111, is. D6, p. 1-16.

Rayburn, J.A., Knuepfer, P.L., and Franzi, D.A., 2005. A series of large, Late Wisconsinan meltwater floods through the Champlain and Hudson Valleys, New York State, USA. Quaternary Science Reviews, v. 24, n. 22, p. 2410-2419.

Reimer, P.J., Bard, E., Bayliss, A., Beck, J.W., et al., 2013. INTCAL13 and Marine13 radiocarbon age calibration curves 0-50,000 years cal BP. Radiocarbon, v. 55, n. 4, p. 1869-1887.

Simms, A., Reynolds, L.C., Bentz, M., Roman, A., Rockwell, T., and Peters, R., 2016. Tectonic subsidence of California estuaries and coasts. Estuaries and Coasts, v. 39, p. 1571-1581.

Sneed, M. and Galloway, D.L., 2000. Aquifer-system compaction: analyses and simulations–the Holly site. Edwards Air Force Base, Anetelope Valley, California. U.S. Geological Survey Water-Resources Investirgations Report 00-4015.

Stanford, S.D., 2010. Onshore record of Hudson River drainage to the continental shelf from the late Miocene through the late Wisconsinan deglaciation, USA: synthesis and revision. Boreas, v. 39, n. 1, p. 1-17.

Stanford, S.D., Miller, K.G., and Browning, J.V., 2015. Coreholes reveal glacial and postglacial history at Sandy Hook. Unearthing New Jersey, v. 11, n. 1, p. 1-6.

Sun, H., Grandstaff, D., and Shagam, R., 1999. Land subsidence due to groundwater withdrawal; potential damage of subsidence and sea-level rise in southern New Jersey, USA. Environmental Geology, v. 37, n. 4, p. 290-296.

Thieler, E.R., Butman, B., Schwab, W.C., Allison, M.A., Driscoll, N.W., Donnelly, J.P., and Uchupi, E., 2007. A catastrophic meltwater flood event and the formation of the Hudson Shelf Valley. Paleogeography, Paleoclimatology, Paleoecology, v. 246, p. 120-136.

Thornton, S.F. and McManus, J., 1994. Application of organic carbon and nitrogen stable isotope and C/N ratios as source indicators of organic matter provenance in estuarine systems: evidence from the Tay Estuary, Scotland. Estuarine, Coastal and Shelf Science. v. 38, i. 3, p. 219-233.

Törnqvist, T.E., Wallace, D.J., Storms, J.E.A., Wallinga, J., Van Dam, R.L., Blaauw, M., Derksen, M.S., Klerks, C.J.W., Meijneken, C., and Snijders, E.M.A., 2008. Mississippi Delta subsidence primarily caused by compaction of Holocene strata. Nature Geoscience, v. 1, p. 173-176.

Traykovski, P., Geyer, R., and Sommerfield, C., 2004. Rapid sediment deposition and fine-scale strata formation in the Hudson estuary. Journal of Geophysical Research, v. 109, i. F2, p. 1-20.

Vereş, D.Ş., 2002. A comparative study between loss on ignition and total carbon analysis on minerogenic sediments. Studia UBB. v. 47, n. 1, p. 171-182.

Woodruff, J.D., Rockwell Geyer, W., Sommerfield, C.K., and Driscoll, N.W., 2001. Seasonal variation of sediment deposition in the Hudson River estuary. Marine Geology. v. 179, p. 105-119.

Yin, J., Schlesinger, M.E., and Stouffer, R.J., 2009. Model projections of rapid sea-level rise on the northeast coast of the United States. Nature Geoscience Letters, v. 2, p. 262-266.